Antifouling Oligoethylene Glycol Functionalized Aromatic Polyamides Brushes Synthesized via Surface-Initiated Chain-Growth Condensation Polymerization

Caleb J. Reese[†], *Yarong Qi*[‡,⊥], *Dustin T. Abele*[†], *Michael J. Wagner*[†], *Xitong Liu*[*,‡], *Stephen G. Boyes*[*,†]

[†]Department of Chemistry, The George Washington University, Washington, DC 20052, USA

[‡]Department of Civil & Environmental Engineering, The George Washington University, Washington, DC 20052, USA

[⊥]Department of Environmental Science, Policy, and Management, University of California, Berkeley, CA, 94720, USA

Keywords: Polymer Brushes, Anti-fouling Surfaces, Aromatic Polyamide, Polyethylene Glycol, Chain Growth Condensation Polymerization, Surface Initiated Polymerization

Abstract

With growing freshwater scarcity in many areas of the world, purifying alternative sources of water such as seawater, brackish water, and wastewater has become increasingly important. One of the main ways this is done is using reverse osmosis (RO) membranes composed of aromatic polyamide films synthesized using interfacial polymerization. These membranes have become the industry standard due to their excellent salt rejection. However, issues with fouling, degradation, and delamination plague current technology, which has led to renewed interest in finding innovative solutions. Polyethylene glycol (PEG) has been used extensively for its antifouling properties and has been incorporated into RO membranes with some success. In this study, oligoethylene glycol (OEG) functionalized aromatic polyamides were covalently grown using surface initiation from silicon wafers, quartz crystal microbalance (QCM) sensors, and silica particles to form high grafting density polymer brushes. Initially, solution-based kinetic studies were used to optimize the polymerization conditions of the OEG functionalized monomers. The optimized conditions were then used for surface-initiated substituent effect chain-growth condensation polymerization of the monomers. The use of these conditions produced uniform OEG functionalized aromatic polyamide brushes with well-defined molecular weight and narrow molecular weight distribution. QCM and atomic force microscopy were used to demonstrate drastically improved antifouling characteristics of the brushes compared with PEG monolayers and aromatic polyamides brushes without the OEG functionalization.

Introduction

Fresh water is among one of the most valued resources for life on earth. With growing population, climate change, and industrialization, this precious resource is becoming scarcer.[1] One

of the biggest causes of this scarcity is contamination of conventional water resources, such as lakes and rivers, from many sources, including municipal, industrial, and agricultural wastewater.[2] To address this problem, nontraditional water sources, like seawater, brackish water, and wastewater, must be tapped into. However, for these water sources to be used as a viable supply of fresh water, they must first be treated and purified until they reach acceptable standards for human consumption and use. One of the leading ways to purify these nontraditional water sources is using membrane processes, of which, reverse osmosis (RO) membranes are the most widely used to remove salts, minerals and contaminates.[3] Of the currently used RO processes, membranes coated with aromatic polyamides are one of the dominant technologies for desalination of seawater.[4] However, these membranes have multiple issues that limit how well they function and their operational lifetimes. One of the main issues that current RO membranes can experience is fouling from small organic molecules, microorganisms, and colloids, all of which lowers the flux through the membrane, decreasing their performance, and increasing the cost of operation for the desalination process.[1,5] One of the conventional ways to address fouling is by adding bleach to degrade the organic molecules in an effort to suppress fouling.[6] The downside of this, however, is that the amide linkages of the conventionally used aromatic polyamide coatings have been shown to deteriorate with exposure to bleach, which also results in a decline of the membrane performance.[7,8] Another issue arises due to the aromatic polyamide layer on RO membranes being traditionally prepared via an interfacial polymerization and, as a result, not being covalently attached to the underlying membrane. This can result in delamination of the coating over time.[4]

One method to address the fouling issue of these membranes is surface modification to introduce anti-fouling functionality. Surfaces that are hydrophilic, contain hydrogen bonding donors, and are electroneutral have been reported to have high resistance to small organic molecules and

microorganisms.[2] A common material that has been used for anti-fouling coatings is PEG.[9] PEG has been used extensively to prevent protein and bacterial adhesion in many applications ranging from biomedical to industrial usage.[10] There are two approaches that have been used to attach PEG or other anti-fouling agents to the cross-linked aromatic polyamide coating of RO membranes; direct covalent attachment and physical attachment. In order to covalently bind PEG or other anti-fouling agents to the aromatic polyamide coating, a polymer or monolayer can be attached to either a secondary amide nitrogen from the polyamide layer, a surface carboxyl group, or can be grown from the polyamide layer using a technique like atom transfer radical polymerization.[2] Physically absorbed coatings are typically produced by soaking the aromatic polyamide membrane in a polymer or antifouling agent solution and then letting the solvent evaporate.[11] When applying physically absorbed coatings, van der Waals attraction, electrostatic interactions, or hydrogen bonding are relied upon to hold the coating modification in place. These forces are not as stable for long term attachment, compared with covalent attachment, making the covalent modification method preferable.[12]

A potential method to overcome many of the issues faced by the current aromatic polyamide RO membranes is the application of polymer brushes. Use of a surface-initiated polymerization approach to prepare aromatic polyamide brushes on a membrane surface would result in a dense, homogenous, and covalently attached film on the membrane. Currently, the crosslinked aromatic films used are relatively thick, at around 200 nm, to remove apertures and surface defects, and possess a high degree of surface roughness because of the interfacial polymerization used to prepare them.[13,14] There is a growing interest in fabricating thinner, smoother polyamide films to enhance water flux and reduce membrane fouling. By directly growing the aromatic polyamide from the membrane surface, in the form of a polymer brush, a covalently attached thin, uniform

layer would be produced, which has the potential to increase water permeability without compromising selectivity.[15,16] The chemistry of the aromatic polyamide brushes can also be highly tailored due to a wide variety of side chains that can be attached to the base monomer unit. One such side chain could be OEG, which would introduce anti-fouling properties to the aromatic polyamide and improve wettability, potentially increasing the membrane flux. Modification of the monomer structure would also allow for a one step synthesis methodology to improve coating stability and introduce anti-fouling properties, instead of the post-polymerization modifications used in current RO membranes.

One recently used method to create polyamide layers similar to that used in RO membranes is molecular layer by layer (mLbL) deposition.[17] mLbL deposition has been shown to create well defined aromatic polyamide films by utilizing a step-growth polymerization technique.[18] This is achieved by reacting di- or tri-functional monomers on the surface one monomer layer at a time.[19] However, this technique has its limitations as a result of having to cycle monomer layers, making this process very time intensive and difficult to scale.[20] Despite this, the reports that have used this technique have shown promising results of increased salt rejection, increased flux, and improved fouling resistance.[16,21-29] Aromatic polyamide brushes could form a similar structure to these films, with the added benefit of a quick, simple, and scalable one step polymerization, but to date aromatic polyamide brushes have not been used to modify RO membranes.

In 2000 Yokozawa et al. demonstrated the conversion of a traditional step-growth polymerization for the solution preparation of aromatic polyamides to a living chain-growth process, termed substituent effect chain-growth condensation (CGC) polymerization.[30] In 2006 Yokozawa further demonstrated the versatility of this technique by preparing aromatic polyamides with OEG side chains in solution.[31,32] These polymers showed very interesting properties, including

reversible phase transitions and improved solubility in water. This groundbreaking work focused on the preparation of aromatic polyamides in solution and did not report on the use of substituent effect CGC polymerization for surface modification, for example, in the preparation of polymer brushes. In 2015 our group published the first example of the synthesis of aromatic polyamides from silica surfaces using substituent effect CGC polymerization.[33] This work demonstrated a proof-of-concept for the adaptation of this new polymerization method for surface modification but was limited in application due to the alkyl chain used as the monomer side chain to improve polymer solubility. Recently, we expanded on our original work by incorporating a protecting side chain on the aromatic polyamide brush to replace the previously used alkyl side chain.[34] The use of a protecting side chain was first demonstrated by Yokozawa in solution polymerizations, as post-polymerization removal of the side chain produces a secondary polyamide structure and allows for the formation of hydrogen bonding, which is responsible for many of the desirable properties of aromatic polyamides.[35] Adaptation of this method using the surface-initiated substituent effect CGC process developed by our group allowed for the formation of thick aromatic polyamide brushes with the protecting side chain, which was removed after polymerization to introduce hydrogen bonding to the polymer brushes. This demonstrated that surface-initiated substituent effect CGC polymerization could be modified to prepare aromatic polyamides with different side chain functionality, and it was hypothesized that it could be used to add OEG side chains to allow for more wettable aromatic polyamide surface and to introduce anti-fouling properties.

In this report, aromatic polyamide brushes with OEG side chains were synthesized via surface-initiated substituent effect CGC polymerization on Stöber silica particles and flat silica substrates. Aromatic polyamides with either para- or meta-substitution along the backbone and OEG side

chains were synthesized, both in solution and as polymer brushes, to compare properties of the final polymers. Kinetic studies were performed in solution to optimize the polymerization conditions and allow for control over the polymer properties. These conditions were then used for the preparation of aromatic polyamide brushes. Quartz crystal microbalance (QCM) and atomic force microscopy (AFM) were used to evaluate the fouling resistance of the polymer brushes and to probe the anti-fouling mechanisms. To the best of our knowledge this is the first example of the synthesis, characterization, and evaluation of surface-initiated aromatic polyamides brushes with OEG side chains.

Experimental section

Materials. All chemicals were purchased from Sigma Aldrich and were used as received unless otherwise noted. N-methylaminopropylmethyldimethoxysilane and 3-[methoxy(polyethyleneoxy)9-12]propyltrimethoxysilane was purchased from Gelest and used as received. HPLC grade tetrahydrofuran (THF) and HPLC grade toluene were purified and dispensed through a MBRAUN MB-SPS solvent purification system. Silicon wafers (prime grade, single side polished) were obtained from Wafer World, with only a native oxide. QCM 5 MHz 14 mm Cr/Au/SiO2 Q Sense sensors were purchased from Quartz Pro. Stöber silica particles were synthesized according to previous work.[34] Bovine serum albumin (BSA, lyophilized powder, ≥98%) was purchased from Sigma-Aldrich.

Characterization. ^{1}H and ^{13}C nuclear magnetic resonance (NMR) spectra were obtained using an Agilent 400-MR DD2 NMR spectrometer. Ellipsometry measurements were carried out on a FS-1 Film Sense multi-wavelength ellipsometer with a 65° angle of incidence. Refractive indices and thickness were measured using a Cauchy model.[36] Infrared spectra were recorded using a Perkin-Elmer Frontier FT-IR Spectrometer using a diamond/ZnSe attenuated total reflectance

(ATR) crystal for bulk samples and a Harrick Scientific VariGATR (glazing-angle ATR) accessory for thin films on silicon wafers. Contact angle measurements were recorded with a ramé-hart standard goniometer 260-U4 using 10 μL drops of deionized water. Images were captured using DROPImage software. A FEI Talos 200 kV with a field-emission source was used to obtain transmission electron microscope (TEM) micrographs. Samples were prepared by dispersing a small amount of material into THF assisted by sonic agitation. An approximately 2 μL aliquot of the mixture was placed on a carbon coated 400 mesh copper grid and allowed to dry for 2 h under vacuum before inserting into the TEM. Thermogravimetric analysis (TGA) was performed on a Perkin-Elmer PYRIS 1 TGA. The samples were placed in a platinum crucible, and then heated in air at a ramp rate of 20 °C/min. Number-average molecular weight (M_n) and polydispersity index (PDI) were measured using a Wyatt miniDawn, Wyatt Optilab, and Agilent HPLC gel-permeation chromatography (GPC) unit (eluent: inhibitor free THF (OmniSolv) with a flow rate of 1.0 mL/min using 5 μm PSS SDV Lux analytical columns: molecular weight range 100–10,000 (1000 A) and 1,000–1,000,000 (100,000 A) g/mol (polystyrene equivalent), respectively). A dn/dc value of 0.09 for polymers between 2,000-10,000 g/mol and 0.12 for polymers over 10,000 g/mol in THF was determined and used for the prepared polymers during the analysis.

The adsorption kinetics of BSA on the polymer brush surfaces were investigated using a QCM (QSense E4 analyzer, Biolin Scientific, Sweden). The polymer brushes were grown on silica coated QCM sensors using the same method as on silicon wafers. The BSA deposition experiments were conducted on polymer brush coated QCM sensors with a flow rate of 0.1 mL/min inside the E4 flow cells at 25 °C. After obtaining a stable baseline (or frequency shift of less 0.2 Hz over 10 min) in a buffer of 10 mM NaCl and 0.4 mM $NaHCO_3$ at pH 7.6 ± 0.2, 50 mg/L BSA dissolved in the same buffer was introduced to the modules to allow for BSA adsorption on the polymer brush

surfaces.[37] The frequency shifts were monitored and converted to the mass of deposition using the Sauerbrey equation.[38] AFM imaging of polymer brushes formed on silicon wafers was performed with a Multimode 8 AFM (Bruker) using a ScanAsyst-Air probe (Bruker). The root-mean-square (rms) roughness of the samples were determined from three replicate measurements. AFM force measurements were obtained by first functionalizing the D cantilever of an NP-O10 AFM probe (Bruker) with a carboxylate-modified latex (CML, Molecular Probes Latex Beads, 4% w/v, diameter 10 μm) sphere. The spring constant of the cantilever was then determined using the thermal noise method.[39] The force measurements between the CML-modified tip and polymer substrates were carried out using the force volume mode in the same buffer solution as in the QCM experiments (i.e., 10 mM NaCl and 0.4 mM $NaHCO_3$, pH 7.6 ± 0.2). The CML-probe was cleaned using ultrapure water and subjected to UV/ozone cleaning for 15–20 min between measurements. The tip was brought to and then pulled off from a surface at a velocity of 500 nm/s, with a dwell time of 1 s.[40] The force measurements were conducted at 30 different locations. The deflection vs displacement curves were converted to force vs separation curves based on the method by Ducker et al. and our previous work.[42-44] The total interaction energy was calculated by integrating the area between the force vs separation curve and the X-axis.[43]

Synthesis

Synthetic procedures for the preparation of the monomers and initiators used in this study can be found in the Support Information.

Solution polymerization of OEG functionalized monomers

The polymerization procedure, utilizing the initiator phenyl 4-(dimethylcarbamoyl)benzoate (DMA-P) and the monomer of interest, is depicted below in **Scheme 1**. Monomer, phenyl 4-((2-

(2-(2-methoxyethoxy)ethoxy)ethyl)amino)benzoate (para-OEG-P-AB) or phenyl 3-((2-(2-(2-methoxyethoxy)ethoxy)ethyl)amino)benzoate (meta-OEG-P-AB), (0.18 g, 0.50 mmol) and the initiator DMA-P (3.4 mg, 0.013 mmol) were placed in a round bottom flask, which was then attached to a Schlenk line under vacuum for 30 min and degassed three times with nitrogen at room temperature. For further drying, 0.25 mL of dry toluene was added to the flask with monomer and initiator. The toluene was then removed at 50 °C on the Schlenk line and the flask refilled with nitrogen. This drying process repeated three times. After drying, anhydrous THF (10 mL) was added to the flask. The flask was placed in a methanol and water mixture cooled with dry ice to -20 °C for 10 min. After this time, 1 M lithium bis(trimethylsilyl)amide (LiHMDS) base (0.60 mL, 0.60 mmol) in THF was rapidly injected and the solution stirred while aliquots were taken for kinetic studies or without sampling for bulk polymers. For the kinetic studies, 2 mL aliquots were withdrawn at given time intervals, either 5 or 15 min. The aliquots for the kinetic studies and the bulk polymerizations were immediately quenched with 5 mL saturated aqueous ammonium chloride after being withdraw or completing the desired polymerization time. The resulting polymer was isolated via extraction with dichloromethane (DCM) and dried over anhydrous $MgSO_4$. The DCM was then removed at room temperature using a rotary evaporator before further drying in a vacuum oven at 60 °C for 2 h. The final polymer was characterized using GPC, NMR spectroscopy, and FTIR spectroscopy.

Deposition of MDMS-Amide-P initiator on flat silica wafers or QCM sensors

Silica wafers cut into 1x2 cm pieces were placed in piranha solution (7 mL ACS reagent sulfuric acid and 3 mL 30% aqueous hydrogen peroxide) at 100 °C for 2 h and subsequently rinsed three times with DI water. QCM sensors were placed in piranha solution for 30 min at room temperature and rinsed three times with DI water. Anhydrous toluene (10 mL) and phenyl

4((3(dimethoxy(methyl)silyl)propyl)(methyl)carbamoyl)benzoate (MDMS-Amide-P) (0.10 g, 0.25 mmol) were added to a straight wall 10 mL reaction flask with cleaned wafers or QCM sensors, which was then capped with a glass stopper. The solution was heated to 100 °C for 2 h without stirring. After this time, the wafers were removed and washed by sonication in fresh toluene twice and THF once, to remove unreacted initiator. Following the washing, the initiator-modified wafers and QCM sensors were annealed in an oven at 140 °C for 30 min and then characterized using ellipsometry, goniometry, and GATR-FTIR spectroscopy.

Deposition of MDMS-Amide-P initiator on Stöber silica

3 g of Stöber silica was placed directly into a 500 mL round bottom reaction flask. Anhydrous toluene (350 mL) and MDMS-Amide-P (0.50 g, 1.20 mmol) were added to the flask, which was then capped with a glass stopper. The solution was heated to 100 °C for 2 h with stirring. After this time, the particles were washed with repeated centrifugation/suspension cycles, twice in toluene and once in THF, using centrifuge tubes. The resulting powder was dried in a vacuum oven at 60 °C for 1 h to give an off-white powder. The initiator-modified particles were characterized using TEM, FTIR spectroscopy, and TGA.

Formation of polymer brushes on flat silicon wafers or QCM sensors

MDMS-Amide-P modified wafers or QCM sensors and a stir bar were placed into a 25 mL round bottom flask along with the desired monomer (para-OEG-P-AB or meta-OEG-P-AB) (0.09 g, 0.25 mmol), and the flask was then sealed with a rubber septum. To fully dry the system, 0.25 mL of dry toluene was added to the flask with monomer and wafer or QCM sensor. The toluene was then removed at 50 °C on the Schlenk line and the flask refilled with nitrogen. The drying process was repeated three times. After drying, anhydrous THF (3 mL) was added to the flask using a degassed syringe. The flask was then placed in a methanol and water mixture cooled with dry ice and

allowed to cool for 10 min at -20 °C. LiHDMS (0.30 mmol, 0.30 mL) was then rapidly added to start the polymerization. The polymerization was allowed to proceed at -20 °C for 6 h. After this time, the flask was unsealed, and the wafers or sensors removed. The polymer formed in solution was then quenched with 5 mL saturated aqueous ammonium chloride solution. The solution polymer was isolated via extraction with DCM and dried over anhydrous $MgSO_4$. The DCM was then removed at room temperature using a rotary evaporator before further drying in a vacuum oven at 60 °C for 2 h. The polymer-modified wafers or QCM sensors were cleaned via sequential sonication in THF three times, and finally dried under a stream of nitrogen. The polymer-modified wafers or QCM sensors were characterized using ellipsometry, goniometry, and GATR-FTIR spectroscopy. Polymer formed in solution was characterized using NMR spectroscopy, FTIR spectroscopy, and GPC.

Formation of polymer brushes on Stöber silica

MDMS-Amide-P modified Stöber silica (0.50 g) and a stir bar were placed into a 25 mL round bottom flask along with the desired monomer (para-OEG-P-AB or meta-OEG-P-AB) (0.36 g, 1.00 mmol), and the flask was then sealed with a rubber septum. To fully dry the system, 0.25 mL of dry toluene was added to flask with the monomer and Stöber silica. The toluene was then removed at 50 °C on the Schlenk line and the flask refilled with nitrogen. The drying process repeated three times. After drying, anhydrous THF (10 mL) was added to the flask using a degassed syringe. The flask was then placed in a methanol and water mixture cooled with dry ice and allowed to cool for 10 min at -20 °C. LiHDMS (1.20 mmol, 1.20 mL) was then rapidly added to start the polymerization. The polymerization proceeded for 6 h before being quenched with 5 mL of saturated aqueous ammonium chloride solution. The polymer-modified Stöber silica was isolated and cleaned by centrifugation and washing with THF three times using plastic centrifuge tubes

and sonication. The final polymer-modified particles were then dried in vacuum oven at 60 °C overnight before characterization with TGA, FTIR spectroscopy, and TEM.

Deposition of PEG monolayer on QCM sensor

Anhydrous toluene (10 mL) and 3-[methoxy(polyethyleneoxy)9-12]propyltrimethoxysilane (0.10 g, 0.61 mmol) were added to a straight wall 10 mL reaction flask with cleaned QCM sensors and capped with a glass stopper. The solution was heated to 100 °C for 2 h without stirring. After this time, the sensors were removed and washed by sonication in toluene twice and THF once, to remove unreacted PEG silane. Following the washing, the PEG monolayer modified QCM sensors were annealed in an oven at 140 °C for 30 min and then characterized using ellipsometry, goniometry, QCM, and AFM.

Formation of meta-substituted deprotected polymer brushes on QCM sensors

The procedure for this polymerization was adapted from our previous study.[34] MDMS-Amide-P modified QCM sensors were placed into a 25 mL round bottom flask along with a stir bar and the monomer (phenyl 3-((4-(octyloxy)benzyl)amino)benzoate) (0.108 g, 0.25 mmol), and the flask was then sealed with a rubber septum. The flask was placed under vacuum for 1 h before being degassed and backfilled with nitrogen three times. After this, anhydrous THF (3 mL) was added to the flask using a degassed syringe. The flask was then placed in a methanol and water mixture cooled with dry ice and allowed to cool for 10 min at -20 °C. LiHDMS (0.3 mmol, 0.3 mL) was then rapidly added using a degassed syringe to start the polymerization. The polymerization was allowed to proceed at -20 °C for 1 h. After this time, the flask was unsealed, and the sensors removed. The polymer-modified sensors were cleaned via sequential sonication in THF, chloroform twice, and THF again, before being finally dried under a stream of nitrogen. To remove the benzyl protecting side chain from the polymer brushes on the QCM sensors, a polymer-

modified sensor was placed in a round bottom flask containing 2 mL of DCM. The flask was sonicated for 10 min, followed by the addition of 2 mL of trifluoroacetic acid (TFA). The flask was then stirred for 72 h at room temperature. After this time, the wafer was removed from the flask, placed in 10 mL of THF, and sonicated for 10 min. The cleaned wafers were then dried in a vacuum oven at 60 °C for 1 h and characterized using ellipsometry, goniometry, QCM, and AFM.

Results and Discussion

Crosslinked aromatic polyamide films have been used extensively for RO membranes due to their ease of synthesis and excellent salt rejection. However, these membranes suffer from issues, such as fouling and film delamination, which limit their lifetime and increase the cost of water purification. Using the recently developed surface-initiated CGC polymerization technique, first reported in our previous work, we hypothesize that by adding a OEG side chain to the monomer used to prepare aromatic polyamide brushes will not only improve the fouling resistance of the polymers but would also allow for covalent attachment of polymers to a wide range of underlying substrates.[33,34]

Substitution of aromatic rings along the backbone of polymer chains has been shown to have a significant effect on a variety of polymer properties, including solubility and a range of physical properties.[34,47] Solubility has always been a challenge with aromatic polyamides due to strong hydrogen bonding and excellent chain packing, particularly for para-substituted monomers, which has resulted in difficulty in processing and application of these polymers.[1] Another property of interest for aromatic polyamides, especially for application in any anti-fouling coating, is resistance to degradation. In RO membranes, meta-substituted aromatic polyamides have shown greater resistance to chemical degradation compared to para-substituted aromatic polyamides and

this, combined with improved flux and salt rejection, have resulted in meta-substituted polyamides being primarily used in film formation for commercial membranes.[49,50] Yokozawa et al. have synthesized both meta- and para-substituted OEG functionalized aromatic polyamides in solution using substituent effect CGC polymerization with low PDI and control over molecular weight but polymerization was limited to solution.[32,46] Using similar synthetic pathways to Yokozawa, both meta-substituted and para-substituted OEG functionalized monomers were synthesized to explore the different characteristics of each in forming polymer brushes.

Monomer and Initiator Synthesis

As mentioned previously, Yokozawa et al. has contributed extensively to CGC aromatic polyamides and, because of this, much of the background on monomer synthesis for this study involved replicating this work. Like Yokozawa, a three OEG repeat unit side chain was chosen as this has been used extensively and has shown good results.[32,46,51-53] However, unlike Yokozawa, the meta-substituted monomer in this study contained a phenoxide leaving group on the ester, as previous work from our group has shown that this leaving group results in enhanced control over the polymerization.[45,54] In short, to synthesize both para- and meta-substituted monomers, 4- and 3-nitrobenzoyl chloride were used as the starting material, respectively. These were reacted with phenol, followed by reduction of the nitro groups with palladium on carbon under a hydrogen atmosphere. The amines were then reacted with 2-[2-(2-methoxyethoxy)ethoxy]acetic acid to form an amide bond, which was selectively reduced using borane THF to give the final monomer structure. The monomers were then purified using column chromatography, resulting in high purity and good yield. Both the surface and solution initiators used in this study were synthesized according to previous work.[34,45]

Solution Polymerizations of the OEG Functionalized Monomers

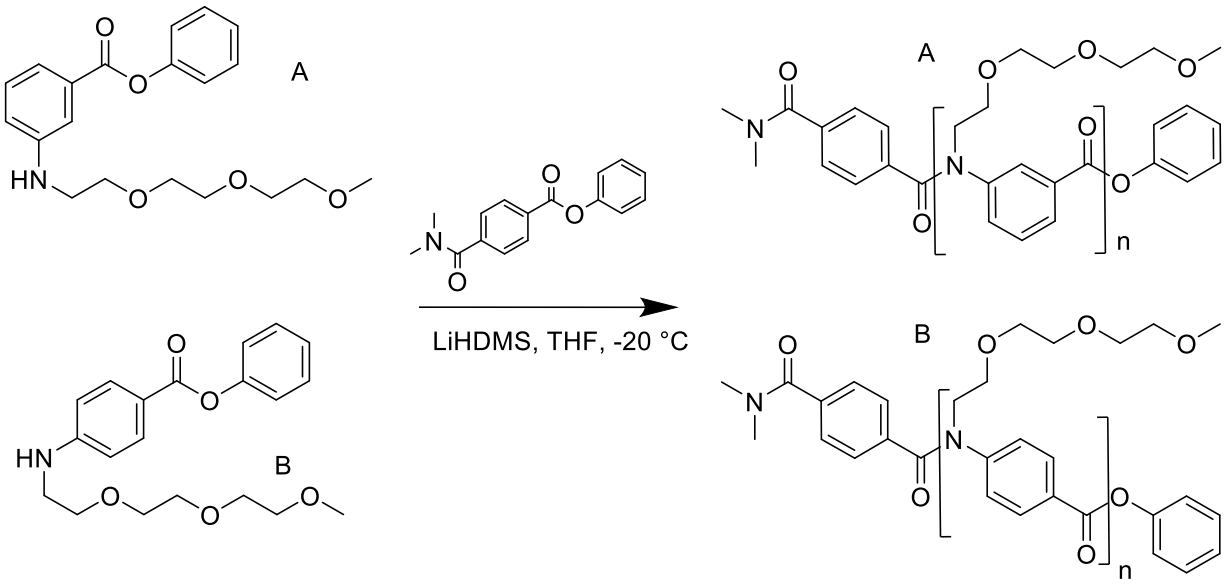

Scheme 1. Synthetic strategy for the solution preparation of meta- (A) and para- (B) substituted OEG functionalized aromatic polyamides using substituent effect CGC polymerization.

Monomer[a]	Drying method[b]	M_n (GPC)	M_w (GPC)	PDI (GPC)	Conversion % (NMR)	M_n[c] (NMR)
Meta OEG	30 min	8,889	10,180	1.15	97	10,485
Meta OEG	Toluene	8,557	9,179	1.07	98	10,653
Para OEG	30 min	10,120	10,620	1.05	80	8,821
Para OEG	Toluene	12,440	12,730	1.02	90	9,737

[a] - Meta OEG - meta-substituted OEG functionalized aromatic polyamide; Para OEG - para-substituted OEG functionalized aromatic polyamide. [b] - 30 min: dried monomer and initiator on Schlenk line for stated time before degassing with nitrogen 3 times, toluene: drying method is outlined in methods and used toluene to azeotropically remove water. [c] - NMR molecular weight found by using the ratio of polymer and initiator NMR peaks. All molecular weights given in g/mol.

Table 1. The effects of drying techniques on the solution polymerization of the meta- and para-substituted OEG functionalized monomers.

Previous work from our research group has demonstrated that the transfer of solution-based substituent effect CGC polymerizations to surface-initiated polymerizations requires a thorough understanding of the polymerization kinetics and optimization of the polymerization conditions.[33,45,54] While Yokozawa et al. have investigated similar monomers to those used in this study previously, those reports did not include detailed polymerization kinetics, the polymerizations for the meta-substituted monomer were only conducted at one temperature, and the meta-substituted monomer had a methoxy leaving group on the ester.[32] In addition, our preliminary work using these OEG functionalized monomer indicated that drying of the monomers played a critical role in their polymerization performance, which has not been previously reported.

During the initial polymerization studies for each of the monomers, it was observed that the results obtained varied significantly when different drying techniques for the monomers were used. PEG polymers have long been known for their affinity to water and, as such, we hypothesized the observed variations could be due to different amounts of water absorbed by the monomers.[55] Water in the substituent effect CGC polymerization solution has the ability to consume the base used to deprotonate monomer, which in turn, effects the overall polymerization, as monomer that is not deprotonated can react with deprotonated monomer to initiate a polymer chain and result in larger PDIs.[44] With this in mind, polymerizations were performed using the same drying technique as previous studies by our group, that is, 30 minutes of drying followed by degassing with nitrogen three times.[34] This was compared to drying by adding toluene and removing it with vacuum three times, and replacing the atmosphere with nitrogen, to remove water azeotropically. After each drying technique, both meta-

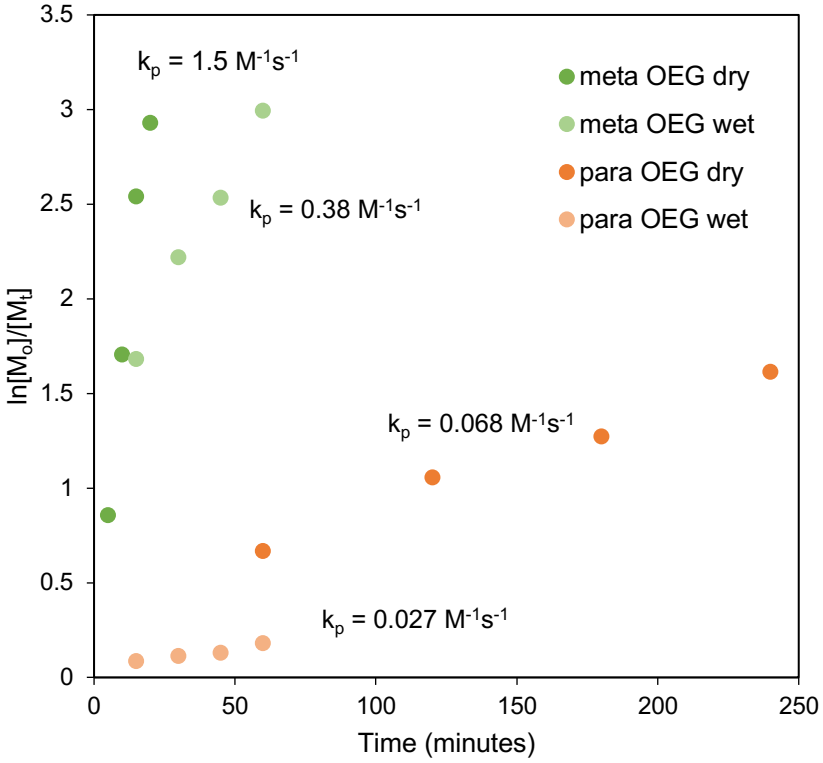

Figure 1. Kinetic plots for polymerization of both meta- and para-substituted OEG functionalized monomers comparing different drying techniques. Wet refers to drying monomer for 30 min and degassing three times. Dry refers to azeotropically removing water three times using toluene.

and para-substituted OEG functionalized monomers were polymerized for 5 h to determine differences in molecular weight, conversion, and PDI (**Table 1**). As Yokozawa had previously reported that -20 °C was the optimal temperature for the para-substituted OEG functionalized monomer, this temperature was utilized for all polymerizations.[46] When comparing the different drying techniques for both monomers it was observed that use of the toluene drying method produced a higher conversion and lower PDI compared to standard drying conditions. These results demonstrate the importance of removing water from the polymerization media when using hydroscopic monomers, such as these OEG functionalized monomers, and the toluene drying method was used for the subsequent surface studies.

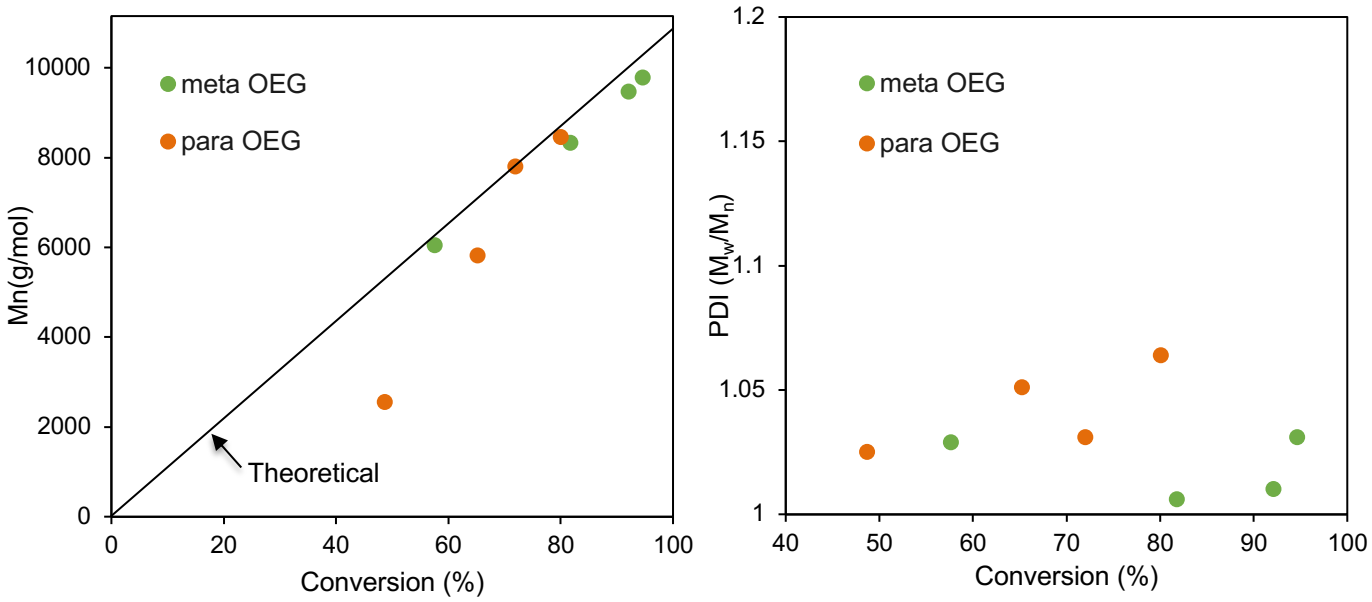

Figure 2. Kinetic plots of M_n (right) and PDI (left) versus conversion for the substituent effect CGC polymerization of meta- and para-substituted OEG functionalized monomers.

The kinetic studies of the OEG-functionalized monomers with the different drying techniques also allowed for the influenced on the polymerization rate to be examined. For both the meta- and

para-substituted OEG functionalized monomers, drying with a toluene azeotrope resulted in a higher rate constant of propagation (k_p), compared to the standard drying technique, while the first order semi-logarithmic plots of conversion versus time remained linear for both drying conditions (**Figure 1**). The k_p differences observed for the different drying conditions demonstrates the importance of maintaining dry conditions during substituent effect CGC polymerizations. The lower k_p values for the standard drying polymerizations, the wet conditions in **Figure 1**, are believed to be due to differences in the rate of addition for protonated monomer compared to deprotonated monomer. The proposed mechanism for substituent effect CGC polymerization relies on deprotonation of the amine on the monomer to deactivate the monomer towards reacting with itself but allow preferential reaction with the initiator or propagating chain.[56] The deprotonated monomer has a negatively charged nitrogen and is more nucleophilic than the protonated monomer, which is a secondary amine. As such, deprotonated monomer will react faster with the carbonyl of the ester on the propagating chain than the protonated monomer. The presence of water in the reaction media will consume some of the added base, resulting in higher concentrations of protonated monomer, which leads to a lowering of the observed k_p.

Like our previous study using monomers with a protecting side chain, polymerizations with the meta-substituted OEG functionalized monomer were faster than with the para-substituted monomer.[34] In this case, the k_p for the toluene azeotrope dried meta-substituted OEG functionalized monomer was 1.5 $M^{-1}s^{-1}$ compared the para-substituted monomer with a k_p of 0.068 $M^{-1}s^{-1}$. This difference is believed to be due to deactivation of the meta-substituted monomer via induction, compared to resonance for the para-substituted monomer, in the substituent effect CGC mechanism resulting in increased reactivity of the carbonyl of the ester. In addition to the semi-logarithmic kinetics plots, M_n and PDI were also monitored with conversion for both the meta-

and para-substituted OEG functionalized monomer that had been dried using the toluene azeotrope (**Figure 2**). For each monomer, the plot of M_n versus conversion demonstrated a close to linear relationship, indicating a constant number of propagating chains, with minimal side reactions. The PDI versus conversion plots demonstrated that both meta- and para-substituted OEG functionalized monomers resulted in polymers with a very low PDI, typically below 1.05, over the course of the polymerization. This is indicative of fast initiation relative to propagation for the polymerization mechanism. It should be mentioned that the conversion ranges for the polymerizations of the meta- and para-substituted OEG functionalized monomers are different due to differences in the k_p values and monitoring the kinetic experiments over similar time increments. As the meta-substituted OEG functionalized monomer has a higher k_p, it will reach higher conversions over a fixed time period when compared to the para-substituted monomer.

While Yokozawa et al. also performed solution studies of these OEG functionalized monomers using substituent effect CGC polymerization, no specific conditions were discussed for drying of the monomers. Instead, their research used additives to try and improve the polymerization of the different monomers, which had trouble with slow polymerization times, low conversion, and self-polymerization.[31,32,46,52,57,58] The hypothesis of Yokozawa et al. was that the poor polymerization performance was due to the ethylene glycol side chains coordinating with the lithium counter ion formed as a result of the LiHDMS base that is used to deprotonate the monomers.[32,46,58] To combat this, different strategies were investigated, including changing reaction temperature and the addition of lithium chloride (LiCl), N,N,N',N'-tetramethylethylene-diamine (TMEDA), crown ether 12-crown-4, or hexamethylphosphoric triamide (HMPA).[31,32,46,52,57,58] While the use of these additives resulted in some improvements, with lower PDI and higher conversions, most of the improvements were not directly compared to the non-additive polymerization or the improvements

were minimal, so it is difficult to fully evaluate the true value of the additive.[31,32,52,57] Based on these reports, and on the work conducted in this study demonstrating the importance of extra drying of the monomer, we concluded that extra drying is the primary means to improve the overall performance of substituent effect CGC polymerizations using OEG functionalized monomers.

Synthesis and Deposition of Silane Based CGC Initiator (MDMS-Amide-P) on Flat Silicon Substrates

After optimization of the solution polymerization conditions, surface-initiated substituent effect CGC polymerization of the meta- and para-substituted OEG functionalized monomers was performed on both flat and high surface area silica surfaces (**Scheme 2**). As with previous work, a silane-based initiator was utilized to allow attachment to silanol groups on the silica surfaces. The MDMS-Amide-P initiator was chosen to match the properties of the solution initiator, while also allowing for a uniform monolayer on the silica surfaces.[34] For flat silica wafers, deposition of the initiator was achieved by first cleaning the surface using piranha solution then placing the wafers in dry toluene with the MDMS-Amide-P initiator and heating to 100 °C for 2 h. The wafers were then sonicated in dry toluene three times to remove any physically absorbed initiator. The initiator-modified surfaces were characterized using techniques like those in previous work and have been shown to confirm the formation of uniform, well defined initiator layers.[34] Using ellipsometry, a thickness of 3.0 ± 0.6 nm was found and agreed with previous work using the same initiator.[34] Measurement of the water contact angle also gave results like those of previous work, with a value 74 ± 2° observed in this case. This indicates a relatively hydrophobic surface when compared to the hydrophilic hydrolyzed silanol surface, with an essentially completely wetted surface, possessing a contact angle of 5-10°. Lastly, the initiator surfaces were characterized using GATR-FTIR spectroscopy and demonstrated a carbonyl ester stretch at 1730 cm^{-1}, amide carbonyl stretch

at 1650 cm^{-1}, and alkyl C-H stretches at 2850 and 2930 cm^{-1}, all of which are characteristic of the initiator structure. These results combined indicate that a well-defined initiator layer was formed from the flat silicon wafers.

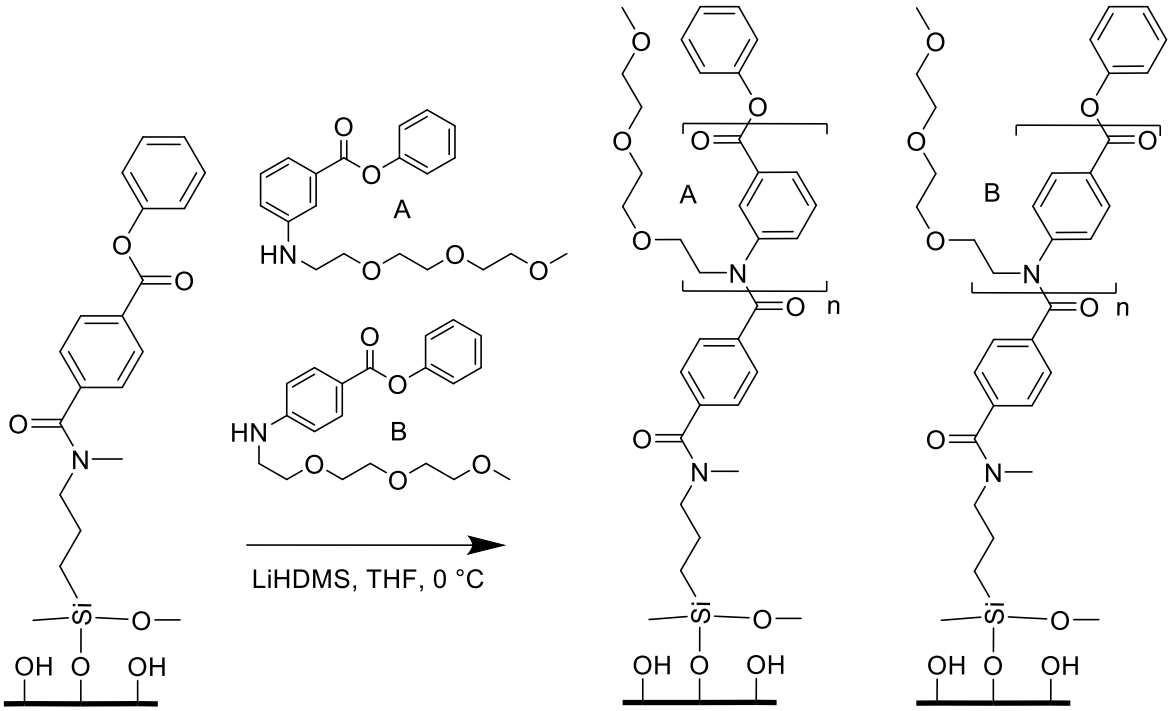

Scheme 2. Surface-initiated substituent effect CGC polymerization for the preparation of a para- (A) and meta- (B) substituted OEG functionalized polymer brushes on flat or curved silica surfaces.

Growth of OEG Functionalized Aromatic Polyamide Brushes from Surface-Immobilized Initiators on Flat Silicon Substrates

Surface-initiated polymerizations of the meta- and para-substituted OEG functionalized monomers were performed by first adding the appropriate monomer and the initiator modified wafer to a reaction flask and degassing. Dry THF was then added, and the reaction flask cooled to -20 °C. The LiHMDS base was then quickly added to start the polymerization (**Scheme 2**). Using

the previously discussed toluene azeotrope drying process, polymer brushes with thicknesses up to 17 ± 2 and 22 ± 4 nm, as measure by ellipsometry, were grown for the para- and meta-substituted OEG monomers, respectively. Using GATR-FTIR spectroscopy on the polymer brushes, the aromatic polyamide structure was confirmed by the presence of an ether stretch at 1130 cm^{-1}, an amide carbonyl stretch at 1645 cm^{-1}, an ester carbonyl stretch at 1710 cm^{-1}, and alkyl C-H stretches at 2910 and 2850 cm^{-1} (**Figure S1**). A broad OH stretch was also seen around 3400 cm^{-1}, which is most likely due to the hydrophilic nature of OEG resulting in atmospheric water absorbing to the surface of the polymer brushes. The water contact angle of the polymer brushes was measured using goniometry and showed a significant decrease from the contact angle of the initiator to values of 49 ± 2° and 47 ± 2° for para- and meta-substituted OEG functionalized polymers, respectively. Comparison of these values to those in our previous study, where the polymer brushes had similar backbone structures but had no OEG side chain on the nitrogen of the amide and gave a contact angle of 95 ± 2°, show that addition of the OEG side chain makes the polymer brushes significantly more hydrophilic.[34] This suggests that not only could these OEG side chains help with the fouling issues of RO membranes but also produce relatively hydrophilic surfaces that would, potentially, also improve the flux of the membrane.

Growth of OEG Functionalized Aromatic Polyamide Brushes from Surface-Immobilized Initiators on High Surface Area Silica

To gain more information about the OEG functionalized aromatic polyamide brushes, high surface area Stöber silica was used to synthesize the polymer brushes. Like our previous study, 500 nm Stöber silica particles were chosen as the high surface area substrate as they mimic the properties of flat wafers but provide a high enough surface area to degraft and collect the surface-grown polymer.[34]

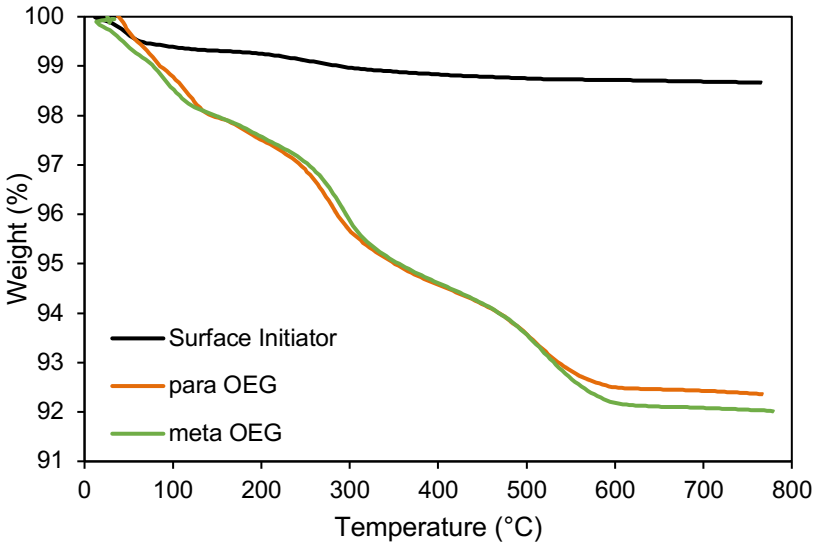

Figure 3. TGA profiles of the MDMS-Amide-P initiator (black) and meta- (orange) and para- (green) substituted OEG functionalized aromatic polyamide brushes on Stöber silica particles.

TGA was used to find the temperature decomposition profiles for the initiator and polymer brush modified silica particles (**Figure 3**). TGA showed a 5.0% weight loss for para-substituted OEG functionalized polymer brush and a 5.5% weight loss for the meta-substituted polymer brush between 200 °C and 600 °C, while the initiator-modified surface showed a 0.5% weight loss in the same range for both systems. Onset degradation temperatures of 243 °C and 478 °C were found for the two degradation stages of the para-substituted OEG functionalized polymer and 263 °C and 485 °C for the meta-substituted OEG functionalized polymer. The first derivative maximums were also used to find the weight loss slope maximums and gave 278 °C and 507 °C for the two degradation stages of the para-substituted OEG functionalized polymer and 296 °C and 530 °C for the meta-substituted OEG functionalized polymer degradation stages. The TGA decomposition profiles for these polymer brushes were like our previous work synthesizing aromatic polyamide brushes without the OEG side chain.[34] The TGA profiles also suggest the presence of water in the polymer brushes due to a small weight loss at around 100 °C of approximately 1.5 wt.% for both polymers, which would be expected due to the hydroscopic nature of the OEG side chains. Next the polymers were cleaved from the silica particles using hydrofluoric acid to determine the grafting density of the polymer

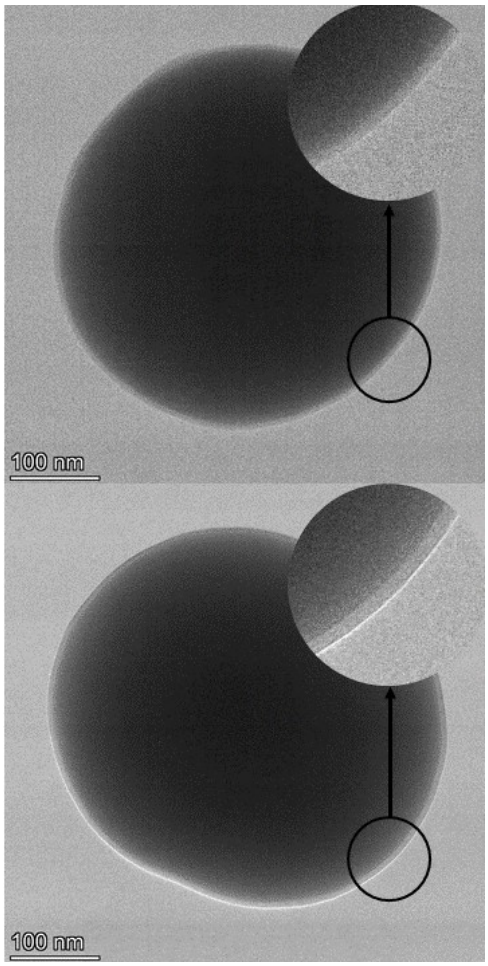

Figure 4. TEM images of the para- (top) and meta- (bottom) substituted OEG functionalized aromatic polyamide brushes grown from Stöber silica particles.

brushes. The degrafted polymers were characterized using GPC to give a M_n of 28,800 g/mol and PDI of 1.27 for the meta-substituted OEG functionalized polymer and a M_n of 24,880 g/mol and PDI for 1.22 for the para-substituted OEG functionalized polymer. Using the molecular weight and the weight loss data, a grafting density of 0.27 chains/nm^2 for meta-substituted polymer brush and 0.28 chains/ nm^2 for the para-substituted polymer brush were calculated using a previously reported technique.[33,34] These values are similar to values previously reported in our studies on the formation of different aromatic polyamide brushes and indicate that the polymers are within the brush regime.[33,34] The degrafted polymers were also characterized using NMR and FTIR spectroscopy. NMR showed the same characteristic peaks observed for the similar solution polymers. FTIR also showed the characteristic ether stretch at 1130 cm^{-1}, amide carbonyl stretch at 1645 cm^{-1}, ester carbonyl stretch at 1710 cm^{-1}, and alkyl C-H stretches at 2910 and 2850 cm^{-1} seen in the solution polymers and the polymer brushes synthesized on the flat substrates.

TEM analysis was used to visually investigate the polymer brushes produced on the silica particles. The TEM micrographs showed uniform coverage on the silica particles for both polymer brush systems, with a thickness of 5.2 ± 0.7 nm for the para-substituted OEG functionalized brush and 5.4 ± 0.8 nm for the meta-substituted OEG functionalized brush (**Figure 4**). In the TEM images, the polymer film is seen as the light gray color compared silica particles being seen as a darker gray color due to lower electron density of the polymer film resulting in less contrast.[59] The uniform coverage is indicative of a well-controlled surface polymerization and suggests that the optimized solution polymerization conditions transferred successfully to the surface.

Anti-fouling performance and mechanisms of OEG functionalized aromatic polyamide brushes

The kinetics of BSA adsorption on the two OEG-functionalized aromatic polyamide brushes was investigated using QCM. As a comparison, we also measured BSA adsorption on sensors coated

with a meta-substituted aromatic polyamide brush with no substitution on the nitrogen (meta H bond) and at similar brush thickness (20 nm) and grafting density (0.28 chains/nm^2), to investigate the effect of OEG functionalization on the aromatic polyamide chain. In addition, sensors coated with a 5 nm PEG (9-12 repeat units) silane monolayer, as a benchmark anti-fouling surface, were also tested. The adsorption of BSA on the surfaces is manifested by negative frequency shifts. The adsorbed BSA layers can be considered rigid with calculated $\Delta D_n/(-\Delta f_n/n)$ values of significantly less than 4×10^{-7} Hz^{-1} (**Table S1**).[60] Therefore, the mass of adsorbed BSA (**Figure 5A and 5B**) can be calculated using the 7th overtone with the Sauerbrey equation (1), where C = 17.7 ng Hz^{-1} cm^{-2} for a 5 MHz quartz crystal, and n is the overtone number.[37,60]

$$\Delta m = -\frac{(C \cdot \Delta f)}{n} \qquad (1)$$

Figures 5 shows that BSA adsorbed on the polymer brush surfaces at different rates, with the measured adsorbed mass over 60 min increasing in an order of meta-substituted OEG functionalized aromatic polyamide brush (meta OEG) < para-substituted OEG functionalized aromatic polyamide brush (para OEG) < PEG monolayer (PEG layer) < meta-substituted aromatic polyamide brush (meta H bond). Following the BSA adsorption experiment, we rinsed the surface with a BSA-free buffer (10 mM NaCl and 0.4 mM $NaHCO_3$ at pH 7.6) for 30 min to study the reversibility of the adsorption. These results show that the change in frequency is negligible during the buffer rinse stage, which indicates that there is almost no release of BSA from the surface after buffer rinse. Therefore, the adsorbed BSA mass presented in **Figure 5b** represents the actual amount of BSA adsorbed on the polymer surfaces with or without buffer rinse. In addition, there is no significant frequency shift during the 10 min prior to BSA adsorption, as well as in the 30-min buffer rinse after BSA adsorption. These results together demonstrate that the polymer coatings on the surfaces are stable and do not detach from the sensor surface in an aqueous

environment. Altogether, these results demonstrate that both the meta- and para-substituted OEG functionalized aromatic polyamide brushes had less BSA adsorption, or were more resistant to BSA fouling, than the PEG monolayer, which is commonly used as a standard for anti-fouling coating. Comparing this PEG monolayer to studies employing similar PEG monolayers and PEG layers with additional functional groups shows similar or less absorbed BSA mass, demonstrating this PEG monolayer was an effective control surface.[61-63] Notably, no BSA adsorption was detected on the meta-substituted OEG functionalized brushes over a period of 60 min, suggesting an excellent resistance to protein fouling. The results also show that the meta-substituted aromatic polyamide brush with no substitution on the nitrogen, used as a comparison to aromatic polyamide coatings commonly used in a range of different membrane technologies, including many RO membranes, had the highest BSA adsorption over the time period. This demonstrates that incorporation of the OEG side chain onto the aromatic polyamide backbone dramatically improves fouling resistance.

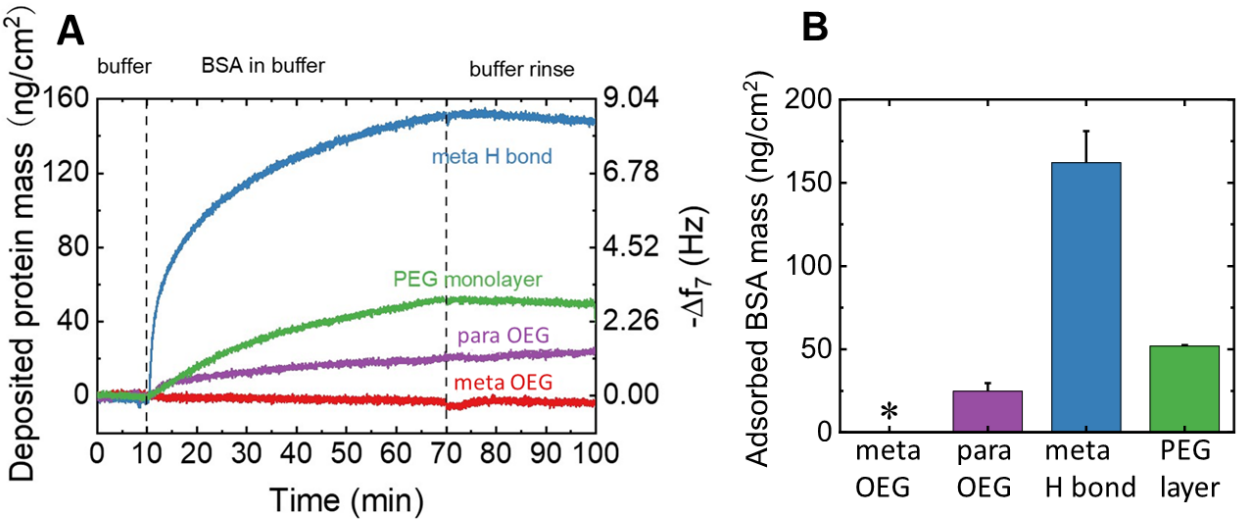

Figure 5. (A) Adsorption of BSA on polymer brush surfaces in a buffer of 10 mM NaCl and 0.4 mM $NaHCO_3$ at pH 7.6. (B) Total adsorbed BSA on the surfaces after 60 min adsorption. Error bars represent standard deviations, n = 2. Asterisk * indicates that adsorption was not detected.

AFM images of the polymer brush surfaces show that the OEG functionalized aromatic polyamide brushes had smoother surfaces at the nanoscale than the meta-substituted deprotected aromatic polyamide brush and PEG monolayer surfaces (**Figure S2**). The lower surface roughness of the OEG functionalized brushes results in more surface area for contact with BSA, which is one possible contributor to the observed less adsorption of BSA on these two surfaces. However, low roughness alone cannot explain the almost zero adsorption of BSA on the meta-substituted OEG functionalized aromatic polyamide brush surface.

To further understand the mechanisms by which the OEG-functionalized aromatic polyamide brushes resist BSA adsorption, the interaction force between the different surfaces and a CML-modified AFM probe, in the same buffer as used in the QCM experiments, was measured (**Figure 6**). The CML colloid was used as a surrogate for BSA because they both carry carboxylic functional groups, which results in similar interactions with the surface.[64,65] In each case, a repulsion was observed when the probe was brought close to the surfaces (**Figure 6**). Notably, the repulsion was stronger and extended to longer distances for the two OEG functionalized aromatic polyamide surfaces compared with meta-substituted deprotected aromatic polyamide brush and PEG monolayer surfaces.

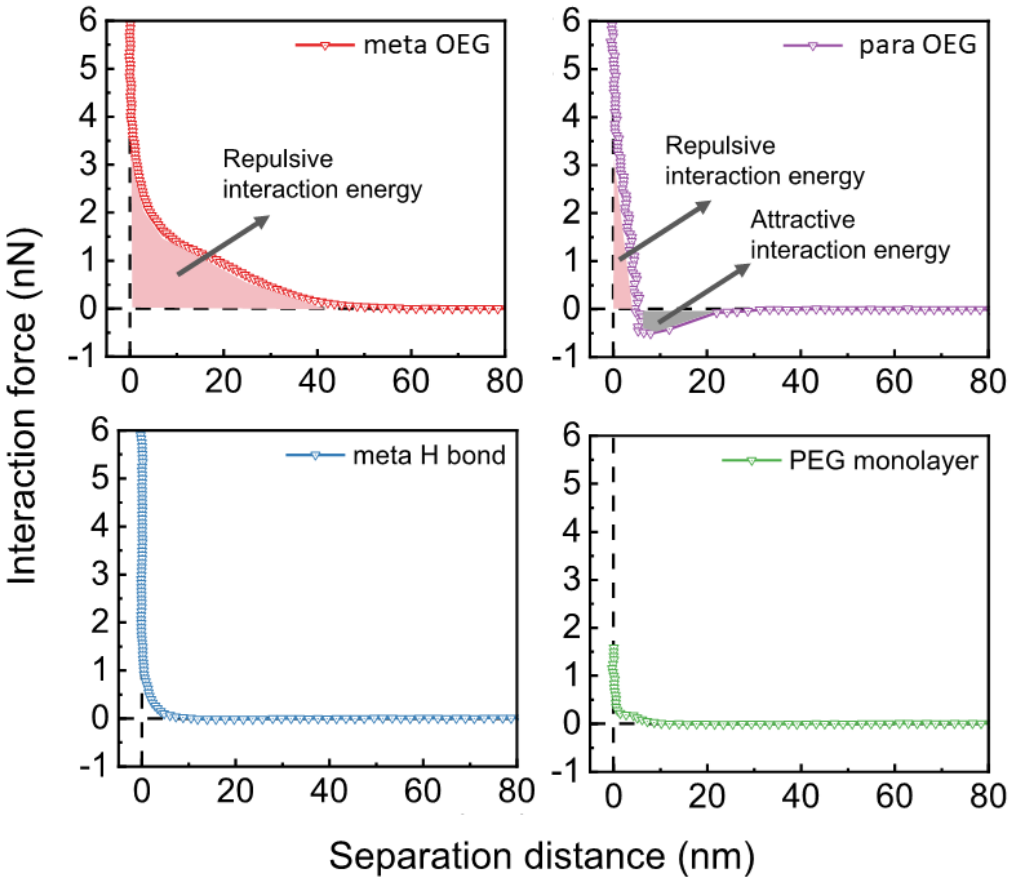

Figure 6. Representative force curves during the approach of the probe to the surface. The shaded regions indicate interaction energy calculated from the area between the force curve and the X-axis.

To better understand these results, the interaction energies for the surfaces were calculated by integrating the areas between the force curves and the X-axis, with positive interaction energy representing repulsion and negative energy representing attraction (**Figure 6**). Because AFM measurement only probes local interactions, 30 force curves were collected at different locations and the distribution of interaction energy is presented in the form of a box plot and frequency plot (**Figure 7**). Both of the OEG functionalized aromatic polyamide surfaces experienced a strong repulsion with the CML probe, while the meta-substituted deprotected aromatic polyamide brush

and PEG monolayer had minimal interaction with the probe (**Figure 7A**). This is more clearly demonstrated in the frequency count plots (**Figure 7B**). Repulsive interactions were detected for 100% of the approach events between the meta-substituted OEG functionalized brush and CML colloidal probe and 80% for the para-substituted OEG functionalized brush. For meta-substituted deprotected aromatic polyamide brush and PEG monolayer, negligible interactions were detected for >90% of the approach events.

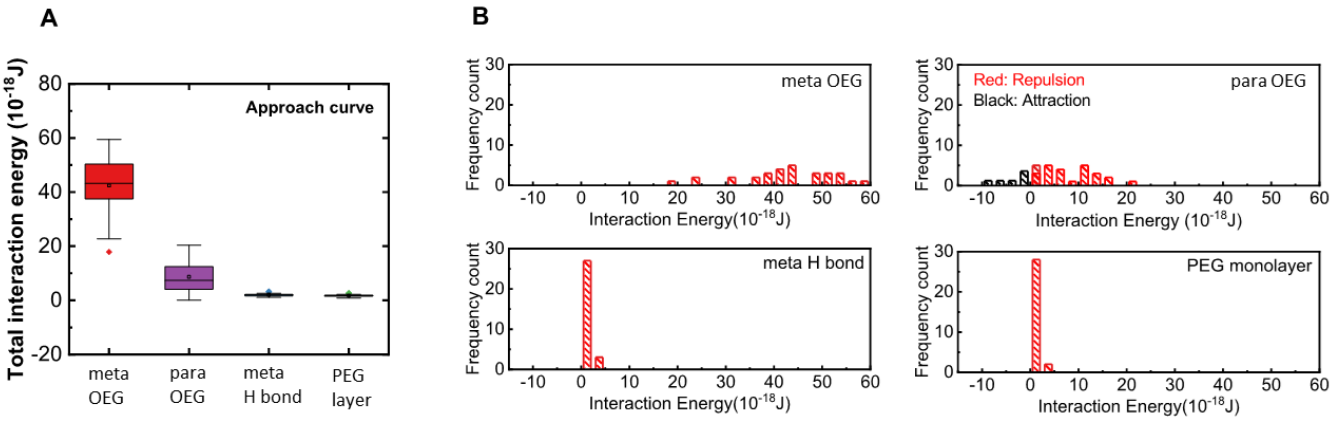

Figure 7. (A) Box plots of total interaction energy calculated from the approach force curves, n = 30. (B) Frequency count of total interaction energy. Red and black bars indicate repulsion and attraction, respectively.

The adsorption of BSA on the OEG functionalized aromatic polyamide brush surfaces can be explained by the interactions measured between the CML probe and the surfaces. The interaction energy was the most repulsive for the meta-substituted OEG functionalized brush surface (**Figure 7A**), corresponding to the observed zero adsorption of BSA. This strong repulsion cannot be electrostatic in nature. The strong repulsion between meta-substituted OEG functionalized brush and the CML probe extended to almost 40 nm (**Figure 6**), well above the Debye screening length of 3 nm at an ionic strength of 10 mM, and also above the dry thickness of the brush (22 nm).[65] Such a long-range repulsive interaction is most likely due to a combination of the steric repulsion

between the CML probe and the brushes, and surface interactions with the OEG side chains on the aromatic polyamide. An "elastic" component of steric repulsion arises when the polymer chains are deformed during the approaching of the CML colloid.[66] In addition to this, the meta-substituted aromatic polyamide chains are more flexible than the para-substituted chains.[67] The enhanced flexibility of the meta-substituted OEG functionalized aromatic polyamide brush potentially allows for increased presentation of the OEG side chains at the polymer-aqueous solution interface. This, combined with the fact that each polymer chain contains multiple OEG side chains, would result in a densely packed, high concentration OEG layer at the interface interacting with the BSA and the CML colloid. Since the PEG layer is hydrophilic, it holds a tightly bound hydration layer at the interface; the compression of this hydration layer will also result in a repulsive force that prevents the adsorption of BSA. As such, the combination of steric repulsion, surface hydrophilicity, and the flexibility of the meta-substituted PEG functionalized aromatic polyamide brushes creates a multi-defense mechanism for resisting the adsorption of BSA. It should be mentioned that the force curve for the para-substituted OEG functionalized aromatic polyamide brush shows the presence of an attractive force for approximately 1/3 of the force measurements (**Figure 6**). This result is somewhat unexpected and is being further investigated using both computational and experimental studies.

Conclusion

Surface-initiated OEG functionalized aromatic polyamides were successfully grown from silicon wafers, QCM sensors, and Stöber silica particles. Before the surface polymerizations were performed, solution polymerizations were studied to ensure a chain-growth behavior and in order to better understand the polymerization mechanism. These studies found that both para- and meta-

substituted OEG functionalized aromatic polyamides maintained control throughout polymerization when the monomers were dried azeotropically with toluene. Polymerizations were then performed on both silicon wafers, demonstrating improved wettability of these surfaces compared to previous studies, and Stöber silica particles, producing grafting densities indicating that these polymer films were in the brush regime. TEM was used to show uniform growth of polymer on the Stöber silica particles. Polymer brushes grown on QCM sensors demonstrated very low protein absorption compared to the two control surfaces, demonstrating the potential these polymers have for antifouling surfaces. Lastly, AFM force measurements suggest that the antifouling properties of the OEG-functionalized polyamide brushes are attributed to the strong steric repulsion between the polymers and foulants and improved flexibility of the meta-substituted brush allowing for easier migration of the OEG side chains to the interface. To the best of our knowledge, this study is the first example of growing OEG functionalized aromatic polyamide brushes from surfaces and the results show that these systems have great promise for application as anti-fouling surface coatings. There is also a great promise in using these OEG-functionalized aromatic polyamide brushes as the separation layer of RO membranes to increase fouling resistance and stability, which will be the focus of a future study.

Associated Content

Supporting information

Initiator and monomer synthesis procedures, table of QCM results, and AFM analysis

Author Information

Corresponding Author *E-mails: sboyes@gwu.edu (S.G.B.), xitongliu@gwu.edu (X. L.)

Notes

The authors declare no competing financial interest.

Author Contributions

The manuscript was written through contributions of all authors. All authors have given approval to the final version of the manuscript.

Funding Sources

SGB and CJR gratefully acknowledge the support of this work by the National Science Foundation under grant CHE MSN #1807863. SGB and XL gratefully acknowledge the support of this work by The George Washington University through the Cross-Disciplinary Research Fund.

Acknowledgements

SGB and CJR gratefully acknowledge the support of this by The George Washington University Chemistry Department. We thank Xun Guan at George Washington University for the analysis of the AFM force measurement data.

Abbreviations

AFM, atomic force microscopy; ATR, attenuated total reflectance; CGC, chain growth condensation; DCM, dichloromethane; DMA-P, phenyl 4-(dimethylcarbamoyl)benzoate; DP, degree of polymerization; FT-IR, Fourier-transform infrared spectroscopy; GATR, grazing-angle attenuated total reflectance; GPC, gel-permeation chromatography; HMPA,

hexamethylphosphoric triamide; LiHMDS, lithium bis(trimethylsilyl)amide; LiCl, lithium chloride; MDMS-Amide-P, phenyl 4-((3-(dimethoxy(methyl)silyl)propyl)(methyl)carbamoyl)benzoate; meta-OEG-P-AB, phenyl 3-((2-(2-(2-methoxyethoxy)ethoxy)ethyl)amino)benzoate; mLbL, MLD, molecular layer deposition; molecular layer by layer; M.p, melting point; NMR, nuclear magnetic resonance; OEG, oligoethylene glycol; para-OEG-P-AB, phenyl 4-((2-(2-(2-methoxyethoxy)ethoxy)ethyl)amino)benzoate; PDI, polydispersity index; PEG, polyethylene glycol; QCM, quartz crystal microbalance; RO, reverse osmosis; TEA, triethylamine; TEM, transmission electron microscope; TEOS, tetraethyl orthosilicate; TGA, thermogravimetric analysis; THF, tetrahydrofuran; TMEDA, N,N,N',N'-tetramethylethylene-diamine.

References

(1) Asadollahi, M.; Bastani, D.; Musavi, S. A. Enhancement of Surface Properties and Performance of Reverse Osmosis Membranes after Surface Modification: A Review. Desalination 2017, 420 (December 2016), 330–383. https://doi.org/10.1016/j.desal.2017.05.027.

(2) Werber, J. R.; Osuji, C. O.; Elimelech, M. Materials for Next-Generation Desalination and Water Purification Membranes. Nat. Rev. Mater. 2016, 1 (5), 16018. https://doi.org/10.1038/natrevmats.2016.18.

(3) Karami, P.; Khorshidi, B.; McGregor, M.; Peichel, J. T.; Soares, J. B. P.; Sadrzadeh, M. Thermally Stable Thin Film Composite Polymeric Membranes for Water Treatment: A Review. J. Clean. Prod. 2020, 250, 119447. https://doi.org/10.1016/j.jclepro.2019.119447.

(4) Lau, W. J.; Lai, G. S.; Li, J.; Gray, S.; Hu, Y.; Misdan, N.; Goh, P. S.; Matsuura, T.; Azelee, I. W.; Ismail, A. F. Development of Microporous Substrates of Polyamide Thin Film Composite Membranes for Pressure-Driven and Osmotically-Driven Membrane Processes: A Review. J. Ind. Eng. Chem. 2019, 77, 25–59. https://doi.org/10.1016/j.jiec.2019.05.010.

(5) Hailemariam, R. H.; Woo, Y. C.; Damtie, M. M.; Kim, B. C.; Park, K. D.; Choi, J. S. Reverse Osmosis Membrane Fabrication and Modification Technologies and Future Trends: A Review. Adv. Colloid Interface Sci. 2020, 276, 102100. https://doi.org/10.1016/j.cis.2019.102100.

(6) Kwon, Y.; Leckie, J. Hypochlorite Degradation of Crosslinked Polyamide Membranes II. Changes in Hydrogen Bonding Behavior and Performance. J. Memb. Sci. 2006, 282 (1–2), 456–464. https://doi.org/10.1016/j.memsci.2006.06.004.

(7) Barassi, G.; Borrmann, T. N-Chlorination and Orton Rearrangement of Aromatic Polyamides, Revisited. J. Membr. Sci. Technol. 2012, 02 (02), 1–4. https://doi.org/10.4172/2155-9589.1000115.

(8) Al-Abri, M.; Al-Ghafri, B.; Bora, T.; Dobretsov, S.; Dutta, J.; Castelletto, S.; Rosa, L.; Boretti, A. Chlorination Disadvantages and Alternative Routes for Biofouling Control in Reverse Osmosis Desalination. npj Clean Water 2019, 2 (1), 2. https://doi.org/10.1038/s41545-018-0024-8.

(9) Liu, S.; Guo, W. Anti-Biofouling and Healable Materials: Preparation, Mechanisms, and Biomedicala Applications. Adv. Funct. Mater. 2018, 28 (41), 1800596. https://doi.org/10.1002/adfm.201800596.

(10) Sanchez-Cano, C.; Carril, M. Recent Developments in the Design of Non-Biofouling Coatings for Nanoparticles and Surfaces. Int. J. Mol. Sci. 2020, 21 (3), 1007. https://doi.org/10.3390/ijms21031007.

(11) Saqib, J.; Aljundi, I. H. Membrane Fouling and Modification Using Surface Treatment and Layer-by-Layer Assembly of Polyelectrolytes: State-of-the-Art Review. J. Water Process Eng. 2016, 11, 68–87. https://doi.org/10.1016/j.jwpe.2016.03.009.

(12) Zhao, D.; Yu, S. A Review of Recent Advance in Fouling Mitigation of NF/RO Membranes in Water Treatment: Pretreatment, Membrane Modification, and Chemical Cleaning. Desalin. Water Treat. 2015, 55 (4), 870–891. https://doi.org/10.1080/19443994.2014.928804.

(13) Lee, K. P.; Arnot, T. C.; Mattia, D. A Review of Reverse Osmosis Membrane Materials for Desalination—Development to Date and Future Potential. J. Memb. Sci. 2011, 370 (1–2), 1–22. https://doi.org/10.1016/j.memsci.2010.12.036.

(14) Al-Hobaib, A. S.; AL-Sheetan, K. M.; Shaik, M. R.; Al-Andis, N. M.; Al-Suhybani, M. S. Characterization and Evaluation of Reverse Osmosis Membranes Modified with Ag_2O Nanoparticles to Improve Performance. Nanoscale Res. Lett. 2015, 10 (1). https://doi.org/10.1186/s11671-015-1080-3.

(15) Culp, T. E.; Khara, B.; Brickey, K. P.; Geitner, M.; Zimudzi, T. J.; Wilbur, J. D.; Jons, S. D.; Roy, A.; Paul, M.; Ganapathysubramanian, B.; Zydney, A. L.; Kumar, M.; Gomez, E. D. Nanoscale Control of Internal Inhomogeneity Enhances Water Transport in Desalination Membranes. Science. 2021, 371 (6524), 72–75. https://doi.org/10.1126/science.abb8518.

(16) Mulhearn, W. D.; Oleshko, V. P.; Stafford, C. M. Thickness-Dependent Permeance of Molecular Layer-by-Layer Polyamide Membranes. J. Memb. Sci. 2021, 618 (June 2020), 118637. https://doi.org/10.1016/j.memsci.2020.118637.

(17) Gu, J.; Lee, S.; Stafford, C. M.; Lee, J. S.; Choi, W.; Kim, B.; Baek, K.; Chan, E. P.; Chung, J. Y.; Bang, J.; Lee, J. Molecular Layer-by-Layer Assembled Thin-Film Composite Membranes for Water Desalination. Adv. Mater. 2013, 25 (34), 4778–4782. https://doi.org/10.1002/adma.201302030.

(18) Reese, C. J.; Boyes, S. G. New Methods in Polymer Brush Synthesis: Non-Vinyl-Based Semiflexible and Rigid-Rod Polymer Brushes. Prog. Polym. Sci. 2021, 114, 101361. https://doi.org/10.1016/j.progpolymsci.2021.101361.

(19) Zhu, Y.; Xie, W.; Gao, S.; Zhang, F.; Zhang, W.; Liu, Z.; Jin, J. Single-Walled Carbon Nanotube Film Supported Nanofiltration Membrane with a Nearly 10 nm Thick Polyamide Selective Layer for High-Flux and High-Rejection Desalination. Small 2016, 12 (36), 5034–5041. https://doi.org/10.1002/smll.201601253.

(20) Choi, W.; Gu, J.-E. E.; Park, S.-H. H.; Kim, S.; Bang, J.; Baek, K.-Y. Y.; Park, B.; Lee, J. S. J.-H. H.; Chan, E. P.; Lee, J. S. J.-H. H. Tailor-Made Polyamide Membranes for Water Desalination. ACS Nano 2015, 9 (1), 345–355. https://doi.org/10.1021/nn505318v.

(21) Xu, G.-R.; Wang, S.; Zhao, H.; Wu, S.; Xu, J.; Li, L.; Liu, X. Layer-by-Layer (LBL) Assembly Technology as Promising Strategy for Tailoring Pressure-Driven Desalination Membranes. J. Memb. Sci. 2015, 493, 428–443. https://doi.org/10.1016/j.memsci.2015.06.038.

(22) Gao, S.; Wang, D.; Fang, W.; Jin, J. Ultrathin Membranes: A New Opportunity for Ultrafast and Efficient Separation. Adv. Mater. Technol. 2020, 5 (4), 1901069. https://doi.org/10.1002/admt.201901069.

(23) Johnson, P. M.; Yoon, J.; Kelly, J. Y.; Howarter, J. A.; Stafford, C. M. Molecular Layer-by-Layer Deposition of Highly Crosslinked Polyamide Films. J. Polym. Sci. Part B Polym. Phys. 2012, 50 (3), 168–173. https://doi.org/10.1002/polb.23002.

(24) Chan, E. P.; Lee, J. H.; Chung, J. Y.; Stafford, C. M. An Automated Spin-Assisted Approach for Molecular Layer-by-Layer Assembly of Crosslinked Polymer Thin Films. Rev. Sci. Instrum. 2012, 83 (11), 114102. https://doi.org/10.1063/1.4767289.

(25) Kwon, S. B.; Lee, J. S.; Kwon, S. J.; Yun, S. T.; Lee, S.; Lee, J. H. Molecular Layer-by-Layer Assembled Forward Osmosis Membranes. J. Memb. Sci. 2015, 488, 111–120. https://doi.org/10.1016/j.memsci.2015.04.015.

(26) Gu, J. E.; Lee, J. S.; Park, S. H.; Kim, I. T.; Chan, E. P.; Kwon, Y. N.; Lee, J. H. Tailoring Interlayer Structure of Molecular Layer-by-Layer Assembled Polyamide Membranes for High Separation Performance. Appl. Surf. Sci. 2015, 356, 659–667. https://doi.org/10.1016/j.apsusc.2015.08.119.

(27) Chan, E. P.; Young, A. P.; Lee, J.-H.; Stafford, C. M. Swelling of Ultrathin Molecular Layer-by-Layer Polyamide Water Desalination Membranes. J. Polym. Sci. Part B Polym. Phys. 2013, 51 (22), 1647–1655. https://doi.org/10.1002/polb.23380.

(28) Chan, E. P.; Lee, S. C. Thickness-Dependent Swelling of Molecular Layer-by-Layer Polyamide Nanomembranes. J. Polym. Sci. Part B Polym. Phys. 2017, 55 (5), 412–417. https://doi.org/10.1002/polb.24285.

(29) Mulhearn, W. D.; Stafford, C. M. Highly Permeable Reverse Osmosis Membranes via Molecular Layer-by-Layer Deposition of Trimesoyl Chloride and 3,5-Diaminobenzoic Acid. ACS Appl. Polym. Mater. 2021, 3 (1), 116–121. https://doi.org/10.1021/acsapm.0c01199.

(30) Yokozawa, T.; Asai, T.; Sugi, R.; Ishigooka, S.; Hiraoka, S. Chain-Growth Polycondensation for Nonbiological Polyamides of Defined Architecture. J. Am. Chem. Soc. 2000, 122 (34), 8313–8314. https://doi.org/10.1021/ja001871b.

(31) Yamazaki, K.; Yokoyama, A.; Yokozawa, T. Solvent and Temperature Effect on Chiral Conformation of Poly(m-benzamide)s. Macromolecules 2006, 39 (7), 2432–2434. https://doi.org/10.1021/ma052712l.

(32) Sugi, R.; Ohishi, T.; Yokoyama, A.; Yokozawa, T. Novel Water-Soluble Poly(m-Benzamide)s: Precision Synthesis and Thermosensitivity in Aqueous Solution. Macromol. Rapid Commun. 2006, 27 (9), 716–721. https://doi.org/10.1002/marc.200600038.

(33) Prehn, F. C.; Boyes, S. G. Surface-Initiated Chain Growth Polyaramid Brushes. Macromolecules 2015, 48 (13), 4269–4280. https://doi.org/10.1021/acs.macromol.5b00957.

(34) Reese, C. J.; Qi, Y.; Abele, D.; Shlafstein, M. D.; Wagner, M. J.; Liu, X.; Boyes, S. G. Aromatic Polyamide Brushes for High Young's Modulus Surfaces by Surface Initiated Chain Growth Condensation Polymerization. Macromolecules 2021 (Accepted with revisions)

(35) Yokozawa, T.; Ogawa, M.; Sekino, A.; Sugi, R.; Yokoyama, A. Chain-Growth Polycondensation for Well-Defined Aramide. Synthesis of Unprecedented Block Copolymer Containing Aramide with Low Polydispersity. J. Am. Chem. Soc. 2002, 124 (51), 15158–15159. https://doi.org/10.1021/ja021188k.

(36) Salazar, Noel B.; Graburn, N. Handbook of Ellipsometry; Elsevier Inc, 2005.

(37) Liu, X.; Chen, K. L. Interactions of Graphene Oxide with Model Cell Membranes: Probing Nanoparticle Attachment and Lipid Bilayer Disruption. Langmuir 2015, 31 (44), 12076–12086. https://doi.org/10.1021/ACS.LANGMUIR.5B02414.

(38) Sauerbrey, G. Verwendung von Schwingquarzen Zur Wägung Dünner Schichten Und Zur Mikrowägung. Zeitschrift für Phys. 1959 1552 1959, 155 (2), 206–222. https://doi.org/10.1007/BF01337937.

(39) Hutter, J. L.; Bechhoefer, J. Calibration of Atomic-force Microscope Tips. Rev. Sci. Instrum. 1993, 64 (7), 1868–1873. https://doi.org/10.1063/1.1143970.

(40) Zhai, H.; Wang, L.; Putnis, C. V. Molecular-Scale Investigations Reveal Noncovalent Bonding Underlying the Adsorption of Environmental DNA on Mica. Environ. Sci. Technol. 2019, 53 (19), 11251–11259. https://doi.org/10.1021/ACS.EST.9B04064.

(41) Qi, Y.; Tong, T.; Liu, X. Mechanisms of Silica Scale Formation on Organic Macromolecule-Coated Surfaces. ACS ES&T Water 2021, 1 (8), 1826–1836. https://doi.org/10.1021/acsestwater.1c00120.

(42) Ducker, W. A.; Senden, T. J.; Pashley, R. M. Measurement of Forces in Liquids Using a Force Microscope. Langmuir 1992, 8, 1831–1836.

(43) Liu, X. Interactions of Silver Nanoparticles Formed in Situ on AFM Tips with Supported Lipid Bilayers. Langmuir 2018, 34 (36), 10774–10781. https://doi.org/10.1021/ACS.LANGMUIR.8B01545.

(44) Qi, Y.; Tong, T.; Liu, X. Mechanisms of Silica Scale Formation on Organic Macromolecule-Coated Surfaces. ACS ES&T Water 2021, 1, (8), 1826–1836.

(45) Prehn, F. C.; Etz, B. D.; Price, D.; Trainor, A.; Reese, C. J.; Vyas, S.; Boyes, S. G. Chain-growth Polycondensation via the Substituent Effect: Investigation into the Role of Initiator and Base on the Synthesis of Poly(N-octyl Benzamide). J. Polym. Sci. 2020, 58 (17), 2407–2422. https://doi.org/10.1002/pol.20200436.

(46) Yoshino, K.; Hachiman, K.; Yokoyama, A.; Yokozawa, T. Chain-Growth Condensation Polymerization of 4-Aminobenzoic Acid Esters Bearing Tri(Ethylene Glycol) Side Chain with Lithium Amide Base. J. Polym. Sci. Part A Polym. Chem. 2010, 48 (6), 1357–1363. https://doi.org/10.1002/pola.23897.

(47) Wang, Y. F.; Sun, J.; Dai, L. X. The Synthesis and Solubility of a Wholly Aromatic Polyamide Containing Para- and Meta-Substituted Phenylene Rings. Appl. Mech. Mater. 2013, 320, 488–494. https://doi.org/10.4028/www.scientific.net/AMM.320.488.

(48) Lin, J.; Sherrington, D. C. Recent Developments in the Synthesis, Thermostability and Liquid Crystal Properties of Aromatic Polyamides. In Polymer Synthesis; Springer-Verlag: Berlin/Heidelberg, 1994; Vol. 111, pp 177–219. https://doi.org/10.1007/BFb0024129.

(49) Roh, I. J.; Park, S. Y.; Kim, J. J.; Kim, C. K. Effects of the Polyamide Molecular Structure on the Performance of Reverse Osmosis Membranes. J. Polym. Sci. Part B Polym. Phys. 1998, 36

(11), 1821–1830. https://doi.org/10.1002/(SICI)1099-0488(199808)36:11<1821::AID-POLB3>3.0.CO;2-T.

(50) Akdag, A.; Kocer, H. B.; Worley, S. D.; Broughton, R. M.; Webb, T. R.; Bray, T. H. Why Does Kevlar Decompose, While Nomex Does Not, When Treated with Aqueous Chlorine Solutions? J. Phys. Chem. B 2007, 111 (20), 5581–5586. https://doi.org/10.1021/jp070586c.

(51) Tanatani, A.; Yokoyama, A.; Azumaya, I.; Takakura, Y.; Mitsui, C.; Shiro, M.; Uchiyama, M.; Muranaka, A.; Kobayashi, N.; Yokozawa, T. Helical Structures of N-Alkylated Poly(p-Benzamide)s. J. Am. Chem. Soc. 2005, 127 (23), 8553–8561. https://doi.org/10.1021/ja0455291.

(52) Ohta, Y.; Kamijyo, Y.; Yokoyama, A.; Yokozawa, T. Synthesis of Well-Defined, Water-Soluble Hyperbranched Polyamides by Chain-Growth Condensation Polymerization of AB_2 Monomer. Polymers (Basel). 2012, 4 (2), 1170–1182. https://doi.org/10.3390/polym4021170.

(53) Yokoyama, A.; Saiki, T.; Masu, H.; Azumaya, I.; Yokozawa, T. Effect of the α-Substituted Chiral Side Chain on the Helical Conformation of N-Substituted Poly(p-Benzamide). Polymer (Guildf). 2018, 134, 175–180. https://doi.org/10.1016/j.polymer.2017.11.066.

(54) Prehn, F. C.; Etz, B. D.; Reese, C. J.; Vyas, S.; Boyes, S. G. Chain-growth Polycondensation via the Substituent Effect: Investigation of the Monomer Structure on Synthesis of Poly(N-octyl-benzamide). J. Polym. Sci. 2020, 58 (17), 2389–2406. https://doi.org/10.1002/pol.20200435.

(55) Alcantar, N. A.; Aydil, E. S.; Israelachvili, J. N. Polyethylene Glycol-Coated Biocompatible Surfaces. J. Biomed. Mater. Res. 2000, 51 (3), 343–351. https://doi.org/10.1002/1097-4636(20000905)51:3<343::AID-JBM7>3.0.CO;2-D.

(56) Yokozawa, T.; Ohta, Y. Transformation of Step-Growth Polymerization into Living Chain-Growth Polymerization. Chem. Rev. 2016, 116 (4), 1950–1968. https://doi.org/10.1021/acs.chemrev.5b00393.

(57) Yoshino, K.; Yokoyama, A.; Yokozawa, T. Synthesis of a Variety of Star-Shaped Polybenzamides via Chain-Growth Condensation Polymerization with Tetrafunctional Porphyrin Initiator. J. Polym. Sci. Part A Polym. Chem. 2011, 49 (4), 986–994. https://doi.org/10.1002/pola.24511.

(58) Ohta, Y.; Kanou, T.; Yokoyama, A.; Yokozawa, T. Synthesis of Well-Defined, Amphiphilic Poly(Ethylene Glycol)-b-Hyperbranched Polyamide. J. Polym. Sci. Part A Polym. Chem. 2013, 51 (17), 3762–3766. https://doi.org/10.1002/pola.26762.

(59) Misof, B.; Roschger, P.; Fratzl, P. Imaging Mineralized Tissues in Vertebrates. Compr. Biomater. 2011, 3, 407–426. https://doi.org/10.1016/B978-0-08-055294-1.00112-4.

(60) Reviakine, I.; Johannsmann, D.; Richter, R. P. Hearing What You Cannot See and Visualizing What You Hear: Interpreting Quartz Crystal Microbalance Data from Solvated Interfaces. Anal. Chem. 2011, 83 (23), 8838–8848. https://doi.org/10.1021/AC201778H.

(61) Xu, B.; Feng, C.; Hu, J.; Shi, P.; Gu, G.; Wang, L.; Huang, X. Spin-Casting Polymer Brush Films for Stimuli-Responsive and Anti-Fouling Surfaces. ACS Appl. Mater. Interfaces 2016, 8 (10), 6685–6692. https://doi.org/10.1021/acsami.5b12820.

(62) Lv, J.; Jin, J.; Han, Y.; Jiang, W. Effect of End-Grafted PEG Conformation on the Hemocompatibility of Poly(Styrene-b-(Ethylene-Co-Butylene)-b-Styrene). J. Biomater. Sci. Polym. Ed. 2019, 30 (17), 1670–1685. https://doi.org/10.1080/09205063.2019.1657621.

(63) Mizrahi, B.; Khoo, X.; Chiang, H. H.; Sher, K. J.; Feldman, R. G.; Lee, J.-J.; Irusta, S.; Kohane, D. S. Long-Lasting Antifouling Coating from Multi-Armed Polymer. Langmuir 2013, 29 (32), 10087–10094. https://doi.org/10.1021/la4014575.

(64) Li, Q. L.; Elimelech, M. Organic Fouling and Chemical Cleaning of Nanofiltration Membranes: Measurements and Mechanisms. Environmental Science and Technology 2004, 38, (17), 4683-4693.

(65) Tang, L.; Gu, W. Y.; Yi, P.; Bitter, J. L.; Hong, J. Y.; Fairbrother, D. H.; Chen, K. L. Bacterial Anti-Adhesive Properties of Polysulfone Membranes Modified with Polyelectrolyte Multilayers. Journal of Membrane Science 2013, 446, 201-211.

(66) Van Oss, C. J., Interfacial Forces in Aqueous Media. CRC press: 2006.

(67) Ohishi, T.; Sugi, R.; Yokoyama, A.; Yokozawa, T. A Variety of Poly(m-Benzamide)s with Low Polydispersities from Inductive Effect-Assisted Chain-Growth Polycondensation. J. Polym. Sci. Part A Polym. Chem. 2006, 44 (17), 4990–5003. https://doi.org/10.1002/pola.21616.

Table of Contents Graphic